Journal of Alloys and Compounds 505 (2010) 43–53

Contents lists available at ScienceDirect

Journal of Alloys and Compounds

journal homepage: www.elsevier.com/locate/jallcom

Combustion synthesis of $MoSi_2$ and $MoSi_2$–Mo_5Si_3 composites: Multilayer modeling and control of the microstructure

F. Baras[a,*], D.K. Kondepudi[b], F. Bernard[a]

[a] Laboratoire Interdisciplinaire Carnot de Bourgogne, UMR 5209 CNRS-Université de Bourgogne, BP 47870, 21078 Dijon Cedex, France
[b] Department of Chemistry, Wake Forest University, Winston-Salem, NC 27109, USA

ARTICLE INFO

Article history:
Received 30 March 2010
Received in revised form 31 May 2010
Accepted 6 June 2010
Available online 15 June 2010

Keywords:
Molybdenum silicides
Powder metallurgy
Self-propagating high-temperature synthesis
Solid–liquid reactions
Kinetics
Modeling

ABSTRACT

In this work, we present a multilayer modeling for the formation of molybdenum silicides in the exothermic reaction between Mo and Si under the influence of a temperature pulse. The heating rate can either be a well-controlled ramp or be generated spontaneously by the propagation of a combustion synthesis front. The model addresses the specific situation above the melting point of silicon and describes the solid–liquid reaction taking place in a single representative particle of molybdenum surrounded by the melt of silicon. We obtain a set of kinetic equations for the propagation of the interfaces between the different layers (Mo/Mo_5Si_3 and $Mo_5Si_3/MoSi_2$) in the solid particle and the change in composition of the melt. This approach enables one to understand the specific microstructure observed during the formation of molybdenum silicides and to assess the role of parameters of combustion synthesis such as the initial size of the particles, the combustion temperature or the stoichiometric coefficient.

1. Introduction

Molybdenum disilicide has recently received considerable attention as a material for high-temperature applications [1–3]. Its properties provide a desirable combination of a high melting temperature (2293 K), high Youngs modulus (440 GPa) [2,4], high oxidation resistance in air [5] or in a combustion gas environment [6], and a relatively low density. However, commercialization of such a compound has been limited because of the low ductility exhibited at room temperature. Consequently, refining grain size to the nanocrystalline level (<100 nm) has been suggested as being a way of improving strength while enhancing ductility and toughness [7]. The second solution is to alloy $MoSi_2$ with other high melting point silicides, like for instance with Mo_5Si_3 [8].

Molybdenum silicides can be synthesized by using different techniques of the powder metallurgy such as hot pressing, reactive sintering, thermal and plasma spray or mechanical alloying [3,9,10]. The large exothermicity of the reaction between Mo and Si powders allows the use of self-propagating high-temperature synthesis (SHS) to produce molybdenum disilicides [11–17]. Such a method is especially attractive because of its high efficiency, short process time and good purification capability with a reduced oxygen contamination compared to conventional processing [18–20].

In the last 10 years, an emerging synthesis route coupling a short duration high-energy ball milling with a self-sustaining reaction has been extensively explored [21–24]. The addition of a mechanical activation step to the SHS process turns out to be a critical improvement, changing the process parameters (e.g. wave velocity) and the nature of the end-product. Although the basic concepts of the SHS method are relatively easy to apply in principle, there remain a number of basic questions related to the physical and to the chemical natures of this phenomenon, as well as, some issues about the phase transformations within the moving combustion front.

Powder processing of silicides implies the spontaneous development of the SHS reaction which is associated with highly exothermic phenomena (up to 3500 K/s [25]). As soon as the system is ignited, the very rapid propagation of combustion front (1–100 mm/s) renders it difficult to control what happens during the combustion synthesis. This is the unavoidable counterpart of low cost and high efficiency. The only way to overcome this intrinsic fact is to determine kinetics and reaction mechanisms during SHS-processing in order to predict the product composition. In this respect, a major challenge is to be able to control the microstructure of the final product as a function of adjustable parameters like green mixture properties or/and combustion temperature, form and speed of the combustion wave.

* Corresponding author. Tel.: +33 3 80 39 61 75; fax: +33 3 80 39 61 67.
E-mail address: fbaras@u-bourgogne.fr (F. Baras).

0925-8388/$ – see front matter © 2010 Elsevier B.V. All rights reserved.
doi:10.1016/j.jallcom.2010.06.024

The kinetic study of siliconized molybdenum wires is especially interesting for understanding the microstructure evolution and its relation to conditions under which synthesis has taken place. Typically the initial sample is a Mo wire of 100 μm in diameter with a thin silicon coating (<10 μm). A bilayer diffusive zone is formed on Mo part consisting of $MoSi_2$ and Mo_5Si_3 phases [26]. Besides this typical solid–solid reaction, the similar experimental study has been performed above the melting point of Si (1414 °C) both in isothermal conditions and under the influence of preheating [27]. By quenching the sample during the process, it is possible to follow the microstructure transformations in this solid–liquid system. A typical situation consists in $MoSi_2$ grains constituting a continuous layer around the Mo core which progressively evolves toward the formation of a compact Mo_5Si_3 layer in-between Mo core and the disilicide. After complete consumption of liquid silicon, a redistribution of the layers occurs with a predominance of molybdenum disilicide. The case of Mo wires rapidly heated above the melting temperature of Si is studied in [28]. Using in situ measurements, it is possible to follow the evolution of the thickness of the diffusion layers and to track the formation of $MoSi_2$ microstructure by recrystallisation.

In SHS experimental studies, the starting material for the synthesis is a fine powder mixture of Mo and Si. The mixture is obtained using a classical turbula mixer for 3 h. Then, the Mo/Si powder mixture is cold-compacted into a cylinder die. Finally, one extremity of the sample is heated to initiate the reaction. Upon ignition, the exothermic reaction is self-sustaining, and a combustion front quickly propagates along the length of the cylinder (10 mm long), converting the green mixture into silicides.

The combustion synthesis of molybdenum disilicide was first investigated by Sarkisyan et al. [11]. The effect of stoichiometry and preheating temperature on the chemical composition of SHS end-products has been studied in [12]. Single-phase $MoSi_2$ is obtained starting from a stoichiometric mixture Mo + 2Si. On the contrary, an atomic mixture 5Mo + 3Si which is supposed to correspond to the Mo_5Si_3 intermetallic compound leads to a multiphase product.

An attempt has been made by Deevi [13] to understand the reaction mechanisms involved in the combustion synthesis of $MoSi_2$ during the propagation of the front. The nature of the mechanism was investigated by correlating the thermal analysis to the time-resolved X-ray identification of the products during the process. At low external heating rate, a situation close to the "natural" propagation case is observed. Indeed, it seems that Mo_5Si_3 is formed first suggesting a solid–solid reaction that occurs in the preheating zone ahead of the reactive combustion zone of the front [13]. But as soon as the local temperature exceeds the melting temperature of Si in less than 2 s the liquid silicon diffuses through the Mo_5Si_3 and an outermost product layer of $MoSi_2$ starts to form. The diffusion of Si towards the inner solid Mo_5Si_3/Mo interface sustains the formation of Mo_5Si_3. Unreacted cores are observed in the reaction products. Similar observations have been reported elsewhere [10,16]. This latter use an IR analysis coupled to time-resolved XRD on synchrotron facilities for determining the combustion synthesis mechanisms of mechanically activated SHS process.

Jo et al. [15] have studied the formation mechanism of $MoSi_2$ by SHS after a quenching of the reacting sample (103 K/s). The microstructure analysis seems to indicate that the formation of $MoSi_2$ operates via dissolution of Mo into Si melt followed by a $MoSi_2$ precipitation. Their conclusions diverge from the usual point of view in which a reaction-diffusion mechanism is suggested. An important issue is to understand the influence of the rapid quenching. The experimental study carried out in [17] on the preparation of $MoSi_2$ and $MoSi_2$–Mo_5Si_3 composites by SHS shows that the stoichiometry of the initial mixture Mo + ξSi significantly influences both the combustion characteristics (propagation mode, front velocity, combustion temperature) and the nature of end-products.

As we have already emphasized, SHS is difficult to control. To be able to use such a processing with confidence, it is essential to establish a direct relationship between the SHS-processing variables and the microstructure of SHS end-products. This would allow evaluating the influence of preheating temperature, green mixture powder size or diluent content both on the morphology and on the chemical composition of the solid. A first attempt in modeling the coupling between the solution of the heat transfer equation and the heterogeneous kinetics was done in [29] to understand the diffusive combustion of multicomponent gasless systems forming multiphase products. In the present work, we have developed a new model which captures the main features of the reactive system and focuses on the structure formation of the synthesized material under the influence of a non-isothermal feedback. On the one hand, the well-documented experimental works offer an excellent background to formulate such a realistic model. On the other hand, a model which accounts for the essential reactive mechanism can become a predictive tool for new experimental investigations. The description of the reaction mechanism leading to a bilayered structure is presented in Section 2 together with the derivation of the equations governing the evolution of the layering structure. The physical properties, the thermodynamic data and the combustion parameters for the Mo + Si system are detailed in Section 3. In Section 4, we present the results of this new approach in various case studies. Finally, the concluding remarks are reported in Section 5 together with the perspectives of the present work.

2. The multilayer modeling

At low temperature, solid–solid interfacial reactions are not favored in a mixture of micrometric Mo and Si powders because of irregular interfaces and voids. The situation is completely different in combustion synthesis. After initiation at one end of the sample, a highly exothermic reaction starts locally. The heat released propagates to the contiguous regions and raises the temperature. Upon the melting of the silicon, the contact area between the two reactants increases dramatically, initiating in turn new seats of combustion which promote the reaction. This mechanism leads to the formation of a reaction front that propagates throughout the system.

2.1. Reactions at interfaces

In this work, we focus on the behavior of a "typical" individual Mo solid grain suspended in the molten Si phase when it experiences a temperature rise due to the propagation of the combustion front (see Fig. 1). As soon as the temperature exceeds the melting threshold, liquid silicon surrounds Mo particles (which are assumed to be spherical for simplicity). During this initial stage, the Mo grain begins to dissolve into the liquid, and at the same time, Si starts to diffuse into the solid particle. A solid solution is forming up to 4% (line 1–2 on the phase diagram, Fig. 2). This first stage is characterized by a mutual dissolution. In a second stage, as the amount of dissolved Si in Mo increases, silicon starts to react with molybdenum to form the intermetallic Mo_5Si_3 (lines 3 and 4, Fig. 2):

$$5Mo(s) + 3Si(l) \rightarrow Mo_5Si_3(s) \quad (1)$$

As a layer of this compound is formed, it surrounds progressively all the solid particle.[1] There is no more direct contact between the

[1] Note that the phase Mo_3Si is not stable in the range of temperature typical of combustion synthesis (1410–1900 °C).

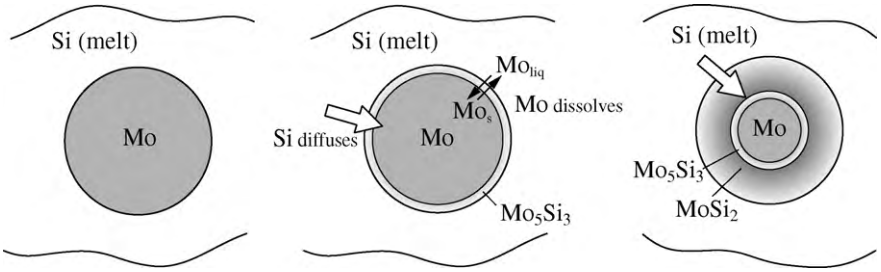

Fig. 1. Different stages of the reaction mechanism between Mo and Si.

solid Mo and the liquid. The inner interface Mo/Mo_5Si_3 is driven out of equilibrium by the sustained diffusion of Si through the Mo_5Si_3 layer. Solid Mo continues to be converted and the thickness of the layers grows as Si diffuses into the solid. At the outer surface, Si may react with the Mo_5Si_3 to form another compound $MoSi_2$ (point 5, Fig. 2), resulting in the growth of a new layer. The reaction reads:

$$Mo_5Si_3(s) + 7Si(l) \rightarrow 5MoSi_2(s) \quad (2)$$

As soon as the layers are formed, there is no direct contact between the solid Mo and the liquid phase but the outermost layer of molybdenum disilicide dissolves into the liquid. The dominant mechanism through which Mo enters the liquid phase is precisely the dissolution of $MoSi_2$ according the reaction:

$$MoSi_2(s) \rightarrow Mo(l) + Si(l) \quad (3)$$

We will neglect the small amount of Mo that might diffuse through the silicides. While the growth of the layers consumes the Si, the amount of Mo in the liquid phase increases until saturation. The final composition of the melt depends on the dissolution rate.

2.2. Modeling

The behavior of the system is conditioned by the reactions at the interfaces. Fig. 3 summarizes the processes occurring at the different locations of the grain. The reaction (1) leading to the formation of Mo_5Si_3 takes place at the interface I. The rate of reaction R_1 at the interface is assumed to be proportional to the chemical affinity of the reaction which can be approximated as the difference between the mole fraction n_1 of Si at this location and its equilibrium value n_{1eq} (see Appendix A):

$$R_1 = k_1 \Delta n_I = k_1(n_1 - n_{1eq}) \quad (4)$$

It is expressed in units of mol m^{-2} s^{-1}. The T-dependent rate constant k_1 is given by the usual Arrhenius law $k_1 = k_{10} \exp(-E/RT)$. As the reaction takes place, Mo is converted to Mo_5Si_3 and the layer begins to propagate inward. The interface is subject to the diffusional flux of Si which feeds the reaction. Since the reaction rate is very rapid at the high temperature, it quickly reaches a value at which it balances the diffusional current of Si, J_1, at interface I. Moreover, we assume that a diffusional quasi-steady state is established rapidly in the system. This allows us to make the approximation:

$$J_1 = 3R_1 \quad (5)$$

which means that the silicon transported by diffusion at the interface is used to form the intermetallic compound.

As soon as the compound Mo_5Si_3 is synthesized, it can itself react with Si to form the disilicide layer. As shown in Fig. 3, the reaction (2) with the formation of $MoSi_2$ occurs at interface II and the reaction rate reads:

$$R_2 = k_2 \Delta n_{II} = k_2(n_2 - n_{2eq}) \quad (6)$$

where the subscript 2 refers to interface II. If we assume that there is no accumulation of matter (due to the rapid reaction), the total diffusional flux of Si at interface II must balance the fluxes and the reaction in the interior interfaces. This leads to the condition:

$$r_2^2 J_2 = r_2^2(7R_2) + r_1^2 J_1 \quad (7)$$

where J_2 is the diffusion current at surface II. At interface III, the outermost layer of $MoSi_2$ may dissolve in Si liquid to form a solution in accordance with the phase diagram. The reaction rate associated

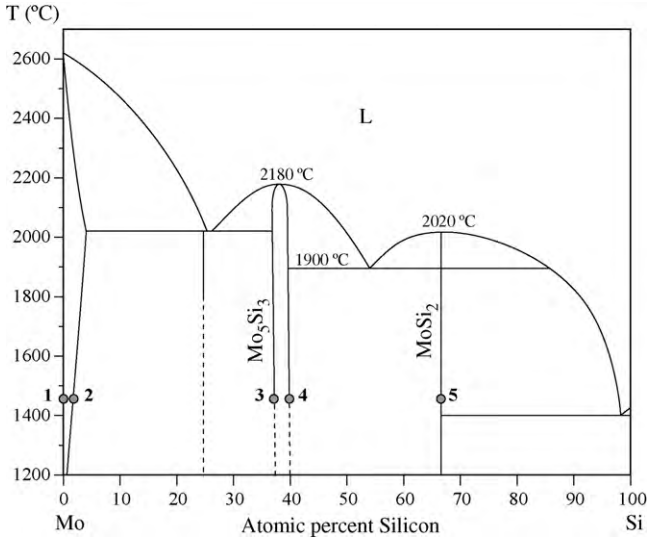

Fig. 2. Phase diagram for the binary system Mo + Si, from [31].

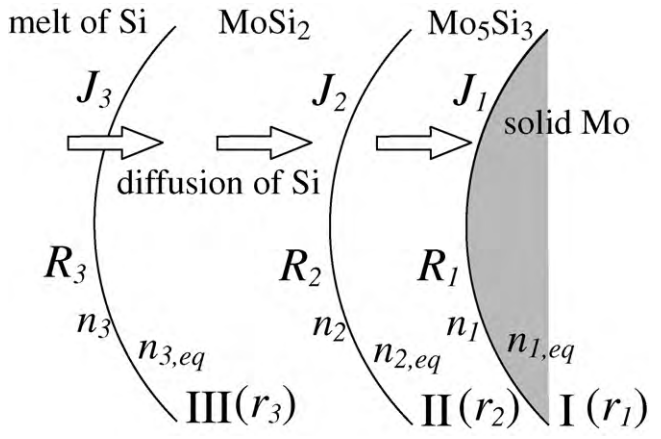

Fig. 3. Slice of the particle during the reaction progress. The kinetics details of the model are represented.

with reaction (3) reads:

$$R_3 = k_2 \Delta n_{III} = k_3(n_3 - n_{3eq}) \tag{8}$$

where the subscript 3 corresponds to interface III. The balance of fluxes on both sides of interface III gives the condition

$$r_3^2 J_3 = r_2^2 J_2 \tag{9}$$

where J_3 is the flux at the external side. The flow of Si at interface III is consumed by the reactions at inner interfaces. Combining Eqs. (5), (7) and (9) gives:

$$r_3^2 J_3 = r_2^2(7R_2) + r_1^2(3R_1)$$

which shows that the flow of Si is consumed by the reactions at interfaces II and III.

2.3. Diffusion

Diffusion transport in solids generally operates though an interdiffusion process [30]. In the Mo–Si system, the situation looks simpler to describe. In several works on the annealing of the diffusion couples $MoSi_2$/Mo at selected temperatures, it has been found that the major diffusing species in the silicides is silicon [26,32,33]. In our modeling, we thus assume that Si is the dominant diffusive element with an effective diffusion coefficient depending on the phase considered.

In this approach we have to estimate the stationary diffusion current of Si, J, at the interfaces of the layers of the spherical particle. For a spherical geometry, one can easily show that the steady-state current can be expressed in terms of the mole fraction of Si at the boundaries (see Appendix B). For instance, we have for the current at the interface I:

$$J_1 = W_{12}(n_2 - n_1) \tag{10a}$$

with

$$W_{12} = D_1 \frac{r_2}{r_1} \frac{1}{r_2 - r_1} \tag{10b}$$

in which D_1 is the diffusion coefficient of Si in the Mo_5Si_3 phase. When $n_2 > n_1$, the diffusion current J_1 is positive which corresponds to a flow toward the center. A similar expression holds for the layer of $MoSi_2$ between interfaces II and III.

2.4. Kinetic equations

With the processes as described above, we are now in a position to write the rate equations for the amount of each substance. In the solid phase, for the number of moles of pure Mo in the inner sphere and for the amount of silicides, $N_{Mo_5Si_3}$ and N_{MoSi_2}, we have

$$\frac{d}{dt} N_{Mo} = -4\pi r_1^2 5R_1 \tag{11a}$$

$$\frac{d}{dt} N_{Mo_5Si_3} = 4\pi r_1^2 R_1 - 4\pi r_2^2 R_2 \tag{11b}$$

$$\frac{d}{dt} N_{MoSi_2} = 4\pi r_2^2 5R_2 - 4\pi r_3^2 R_3 \tag{11c}$$

In the liquid phase, for the number of moles N'_{Mo} of Mo and N'_{Si} of Si, we have

$$\frac{d}{dt} N'_{Mo} = 4\pi r_3^2 R_3 \tag{12a}$$

$$\frac{d}{dt} N'_{Si} = 4\pi r_3^2(-J_3 + 2R_3) \tag{12b}$$

It is easy to check that the conservation of Mo and Si is satisfied by the set of Eqs. (11) and (12):

$$\frac{d}{dt}(N'_{Mo} + N_{MoSi_2} + 5N_{Mo_5Si_3} + N_{Mo}) = 0$$

$$\frac{d}{dt}(N'_{Si} + 2N_{MoSi_2} + 3N_{Mo_5Si_3}) = 0$$

Since our final goal is to compare the predictions of the model to experimental data, it would be more appropriate to introduce the radii of the interfaces. Eq. (11) can be expressed easily in terms of r_1, r_2 and r_3 by noting that

$$N_{Mo} = \frac{1}{V_{mMo}} \frac{4\pi}{3} r_1^3$$

$$N_{Mo_5Si_3} = \frac{1}{V_{m12}} \frac{4\pi}{3}(r_2^3 - r_1^3)$$

$$N_{MoSi_2} = \frac{1}{V_{m23}} \frac{4\pi}{3}(r_3^3 - r_2^3)$$

where V_{m12} and V_{m23} are the molar volumes of the Mo_5Si_3 and $MoSi_2$ phases, respectively. The complete nomenclature of the model is listed in Appendix C. The next task is to make a set of closed equations in $\{r_1, r_2, r_3, N'_{Mo}, N'_{Si}\}$ from Eqs. (11) and (12) which takes into account the relations (4)–(9) and expression (10). This can be done following the method presented in a previous publication (see Ref. [34] for details). Applying this method of calculation to the present system, we obtain a closed set of equations as outlined below. First, the following functions of system variables are defined:

$$W_{12} = D_1 \frac{r_2}{r_1} \frac{1}{r_2 - r_1} \tag{13a}$$

$$W_{23} = D_2 \frac{r_3}{r_2} \frac{1}{r_3 - r_2} \tag{13b}$$

$$\Gamma = \frac{r_1^2}{r_2^2} \frac{3k_1 W_{12}}{3k_1 + W_{12}} \tag{13c}$$

The mole fractions of Si at interfaces III and II take the explicit form:

$$n_3 = \frac{N'_{Si}}{N'_{Si} + N'_{Mo}} \tag{13d}$$

$$n_2 = n_{2eq} + \frac{W_{23}(n_3 - n_{2eq}) - \Gamma(n_{2eq} - n_{1eq})}{7k_2 + W_{23} + \Gamma} \tag{13e}$$

With these definitions, the reaction rates R_1, R_2, and R_3, at the interfaces I, II and III respectively (see Fig. 3), can be written as

$$R_1 = k_1 \frac{W_{12}}{3k_1 + W_{12}}(n_2 - n_{1eq}) \tag{13f}$$

$$R_2 = k_2 \frac{W_{23}(n_3 - n_{2eq}) - \Gamma(n_{2eq} - n_{1eq})}{7k_2 + W_{23} + \Gamma} \tag{13g}$$

$$R_3 = k_3(n_3 - n_{3eq}) \tag{13h}$$

With the reaction rates thus specified, the following closed set of equations that describe the propagation of interfaces, as specified by r_1, r_2, r_3, and the composition of the surrounding liquid, as specified by N'_{Mo} and N'_{Si} are obtained:

$$\frac{dr_1}{dt} = -V_{mMo} 5R_1 \tag{14a}$$

$$\frac{dr_2}{dt} = \frac{r_1^2}{r_2^2}(V_{m12} - 5V_{mMo})R_1 - V_{m12}R_2 \tag{14b}$$

Table 1
Physical properties of Mo, Si and silicides as reported in the literature.

Property	Si	Mo	Mo_3Si	Mo_5Si_3	$MoSi_2$
Molar mass ($kg\,mol^{-1}$)	0.02808	0.09594	0.3159	0.56394	0.1521
Density ($kg\,m^{-3}$) $\times 10^{-3}$ [35]	2.33	10.22	8.97	8.26	6.24
Molar volume ($m^3\,mol^{-1}$) $\times 10^5$ [35]	1.21	0.94	3.52	6.83	2.42
Melting T (K)	1683	2890		≈2445	≈2287
Heat of formation ΔH_{for} ($kJ\,mol^{-1}$) [13]			100.46	841.39	262.88

$$\frac{dr_3}{dt} = \frac{r_1^2}{r_3^2}(V_{m12} - 5V_{m\mathrm{Mo}})R_1 + \frac{r_2^2}{r_3^2}(5V_{m23} - V_{m12})R_2 - V_{m23}R_3 \quad (14c)$$

$$\frac{dN'_{\mathrm{Mo}}}{dt} = (4\pi r_3^2)R_3 \quad (14d)$$

$$\frac{dN'_{\mathrm{Si}}}{dt} = -(4\pi r_2^2)7R_2 - (4\pi r_1^2)3R_1 + (4\pi r_3^2)2R_3 \quad (14e)$$

The first term on the right-hand side of Eq. (14b) represents the change in r_2 due to change in volume when Mo converts to Mo_5Si_3 upon reacting with Si. Again, the first two terms on the right-hand side of Eq. (14c) represent the change in r_3 due to change in volume due to the conversion of Mo to Mo_5Si_3 and Mo_5Si_3 to $MoSi_2$.

In some cases, the reaction rates at the interfaces may become very large causing the evolution to be diffusion limited. Large reaction rates means:

$$k_1 \gg W_{12} \quad \text{and} \quad k_2 \gg W_{23}, W_{12} \quad (15)$$

This leads to the following approximations for the functions and variables introduced previously (Eqs. (13)):

$$\Gamma = \frac{r_1^2}{r_2^2}W_{12} \quad (16a)$$

$$n_2 \approx n_{2eq} \quad (16b)$$

$$R_1 = \frac{W_{12}}{3}(n_2 - n_{1eq}) = \frac{W_{12}}{3}(n_{2eq} - n_{1eq}) \quad (16c)$$

$$R_3 = \frac{1}{7}[W_{23}(n_3 - n_{2eq}) - \Gamma(n_{2eq} - n_{1eq})] \quad (16d)$$

The set of nonlinear Eq. (14) with relations (13) or (16) complete the formulation of the multilayer modeling. The numerical solution gives the evolution of layers radii and the composition of the melt for a given temperature field. Our modeling includes a limited number of parameters whose values are discussed in the next section.

3. Physical properties and thermodynamic data for the Mo + Si system

In order to obtain realistic values of the layer growth, we have collected the available data for the Mo + Si system. If some information is missing, we make reasonable assumptions to have a physically meaningful result. The main physical properties, like molar volume or melting temperature, of Mo, Si and silicides are summarized in Table 1.

To compute the equilibrium values of the mole fractions n_{1eq} and n_{2eq} (which are approximated to be the activities), we use the temperature-dependent molar Gibbs energies of formation, ΔG_f, of the compounds Mo_5Si_3 and $MoSi_2$. In the range of temperature from 1600 to 3000 K, these energies are expressed as[2]:

$$\mathrm{I}: 5\mathrm{Mo} + 3\mathrm{Si}(\text{in the liquid phase}) \rightarrow \mathrm{Mo_5Si_3}$$

$$\Delta G_{f\mathrm{I}}(\mathrm{Mo_5Si_3})[\mathrm{kJ\,mol^{-1}}] = -428.75 + 0.04984T + 9.505 \times 10^{-6}T^2$$

$$\mathrm{II}: \mathrm{Mo_5Si_3} + 7\mathrm{Si} \rightarrow 5\mathrm{MoSi_2}$$

$$\Delta G_{f\mathrm{II}}(\mathrm{MoSi_2})[\mathrm{kJ\,mol^{-1}}] = -1430.81 + 0.048657T - 7.4702 \times 10^{-7}T^2$$

At equilibrium, at the interface I, we have:

$$\frac{a(\mathrm{Mo_5Si_3})_{eq}}{a(\mathrm{Mo})_{eq}^5 a(\mathrm{Si})_{eq}^3} = K_{eq} = \exp\left(\frac{\Delta G_{f\mathrm{I}}}{RT}\right)$$

If the activities $a(Mo_5Si_3)_{eq}$ and $a(Mo)_{eq}$ are known, then $a(Si)_{eq} = a_{1eq}$ can be calculated using this expression. By approximating the activities of the pure solids to 1 and the activity of Si in the Mo_5Si_3 phase by the mole fraction, n_{1eq}, we obtain an approximate value of equilibrium mole fraction as a function of the temperature.

$$n_{1eq} \approx (\exp(\Delta G_{f\mathrm{I}}))^{1/3} \quad (17a)$$

In the outer layer, Si is dissolved in solid $MoSi_2$ and diffuses towards the interface II. At equilibrium, we get:

$$\frac{a(\mathrm{MoSi_2})_{eq}}{a(\mathrm{Mo_5Si_3})_{eq}^{1/5} a(\mathrm{Si})_{eq}^{7/5}} = K_{eq} = \exp\left(\frac{\Delta G_{f\mathrm{II}}}{RT}\right)$$

$$n_{2eq} \approx (\exp(\Delta G_{f\mathrm{II}}))^{5/7} \quad (17b)$$

Note that in the temperature range of interest [1700–2100 K], the estimated values of $a(Si)_{eq} \ll 1$ at interface I and never exceeds 0.16 at interface II. It is thus justified to approximate $a(Si)_{eq}$ with mole fractions (see Appendix A).

Several experimental investigations have been devoted to diffusion in silicides. As shown in a study on the reaction and diffusion in the Mo-Si system by ZrO_2 marker experiments, it appears that the dominant diffusing element in the $MoSi_2$ and Mo_5Si_3 silicides is the silicon [32]. The silicon diffusivity in the Mo_5Si_3 has been studied within the temperature interval [1473 – 2073 K] in [33] at isothermal annealing of the $MoSi_2$/Mo diffusion couple. Since the growth kinetics of the Mo_5Si_3 intermediate layer obeys a parabolic law within this temperature range, it is possible to give an estimate of the solid-phase diffusion coefficient of silicon in the Mo_5Si_3 silicide:

$$D_f = 38.6 \times 10^{-4}\exp\left(\frac{-E_d}{RT}\right) \ (\mathrm{ms^{-1}}) \quad \text{with} \quad E_d = 309\,\mathrm{kJ\,mol^{-1}} \quad (18)$$

[2] The temperature-dependent Gibbs energy of formation has been calculated using the online calculator FACT (facility for the analysis of chemical thermodynamics for treating thermodynamic properties and calculations in chemical metallurgy) developed by the Ecole Polytechnique and Mc Gill University (Canada). See http://www.crct.polymtl.ca/FACT/. If more accurate data on this system is available, it could easily be included in this model.

Nevertheless, the determination of the diffusion activation energy E_d seems to be a delicate problem since there exist various estimates ranging from $E_d = 209\,\mathrm{kJ\,mol^{-1}}$ [37,38] to $E_d = 350\,\mathrm{kJ\,mol^{-1}}$ [39]. This important discrepancy seems to be reduced within a lower temperature range. Another important aspect which has been established in these various studies is the fact that the diffusion coefficient of Si in the $MoSi_2$ (D_2) layer is significantly larger than it is the Mo_5Si_3 (D_1) layer. In the numerical study of the multilayer modeling (Section 4), we will use these estimated values for the diffusion coefficient of Si in the different phases. This will allow us to understand the influence of the diffusive transport of silicon on the formation of silicides.

The rate constants k_1, k_2 for the reactions at interfaces I and II are difficult to estimate. We can use the typical values given for the formation of an intermetallic [40]. The comparative analysis of Eqs. (14) with (13) and Eqs. (14) with (16) shows that large reaction rates have a negligible influence on the layers formation which is mainly dominated by the diffusion processes. For the rate of dissolution at the interface of the outermost layer into the surrounding liquid, we may use:

$$R_3 = k_0 \exp\left(\frac{-E_3}{RT}\right)(n_3 - n_{3eq})$$

in which the preexponential factor $k_0 = 20\,\mathrm{mol\,m^{-2}}$ and the activation energy $E_3 = 76\,\mathrm{kJ\,mol^{-1}}$ [34]. As $MoSi_2$ layer dissolves in the melt, the mole fraction of Si decreases and the solution approaches the dissolution equilibrium. The equilibrium value of the Si mole fraction, n_{3eq}, can be obtained from the phase diagram. For the Mo–Si system, the temperature dependence of the equilibrium Si mole fraction in the melt is approximated by

$$n_{3eq} = 9.2355 - 0.012535T + 6.4475 \times 10^{-6}T^2 - 1.1335 \times 10^{-9}T^3$$

For predicting the time-varying composition of the system, we have to specify the temperature field to which each individual grain is submitted. The simplest case is to keep the temperature constant or to impose a linear ramp. But for a typical SHS reaction, the temperature profile is much more complex [25,41]. Ahead of the reaction front, the temperature shows an exponential behavior dominated by the conduction of the heat produced by the reaction. In the reaction zone, the observed abrupt variation corresponds to the ignition of the exothermic reaction. Finally, after reaching its maximum value (adiabatic or combustion temperature), the temperature decreases exponentially with a characteristic time associated to the cooling.

We have collected available data for describing a realistic temperature pulse which exhibits the same features as those observed in SHS experiments. The expected adiabatic temperature for a stoichiometric mixture Mo + 2Si is about 1927 K. The heating rate in the reaction zone has been reported in the literature and is estimated to $800\,\mathrm{K\,s^{-1}}$ in [13] and to $1230\,\mathrm{K\,s^{-1}}$ in [36] which are well in the usual range of $10^4 - 10^6\,\mathrm{K\,s^{-1}}$. The overall temperature pulse takes about 8 s, rising from and returning to a reference temperature of 1500 K. In the framework of our model, we will consider the temperature profile above the melting of Si (1683 K) since we suppose that the reaction starts with the melting of the silicon. When both components are solids, the reaction rate is virtually zero [13]. A reasonable choice for describing the increase in T in a typical SHS is given by the following expression:

$$T(t) = T_0 + \frac{A\exp(\alpha t)}{B + \exp(\beta t)} \tag{19}$$

with $T_0 = 1710$ K, $A = 350$, $B = 100$, $\alpha = 12$ and $\beta = 12.7$. The temperature rapidly reaches a maximum of $T_{max} = 1929$ K with a heating rate of $d_tT = 776\,\mathrm{K\,s^{-1}}$ before slowly decreasing. The temperature profile the system is subjected to in our simulations is shown in Fig. 4 for two values of the parameter β.

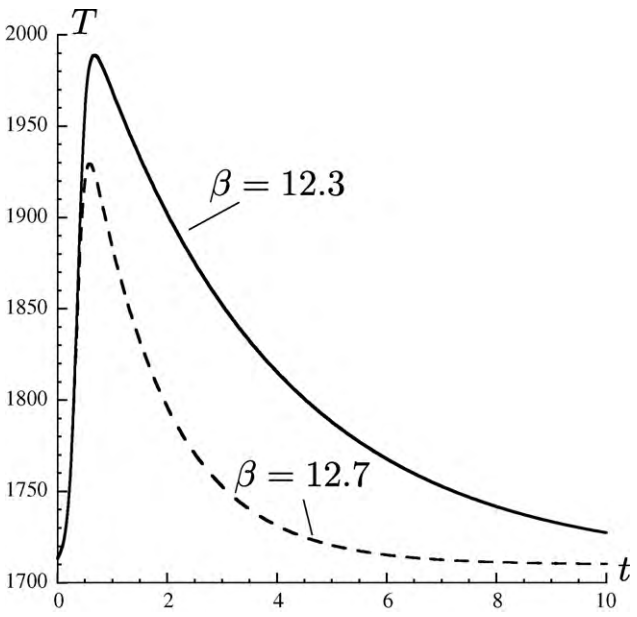

Fig. 4. Temperature profile that the system is subjected to in the simulation. Component Mo melts at 2890 K and Si at 1683 K. This temperature simulates a condition in which particles of Mo are surrounded by Si liquid. We see the influence of parameter β in Eq. (19) on the maximum temperature reached and on the cooling rate, with other parameter values in Eq. (19) $T_0 = 1710$ K, $\alpha = 12$, $A = 350$, $B = 100$. The temperature is measured in K, and time, in seconds.

4. Results and discussion

In this section, we present the numerical study of two-layer model described by Eqs. (14) with the relations (16) corresponding to the limit of large reaction rates. The values of the parameters for the Mo + Si system have been discussed in the previous section.

The initial size r_0 of the Mo particle is used as the length scale so that r_1, r_2 and r_3 are in units of r_0. We suppose that there is initially a very thin layer of the two silicides surrounding the Mo particle. These nano-layers act as a "uniform" seed for the formation of the silicides. Thus the initial conditions are: $r_1(t=0) = 1$; $r_2(t=0) = 1 + \delta$; $r_3(t=0) = 1 + 2\delta$ where δ is a small

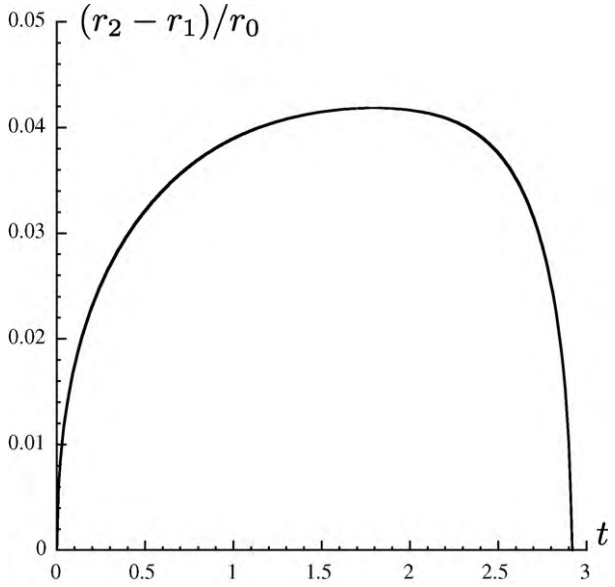

Fig. 5. Time evolution of the Mo_5Si_3 layer thickness for a constant temperature field, $T = 1900$ K. Time is measured in seconds.

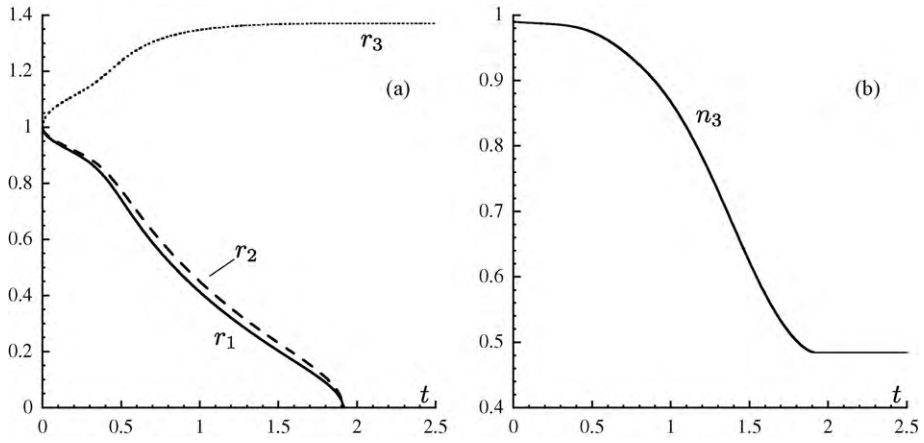

Fig. 6. Results of simulation with a SHS temperature pulse shown in Fig. 4, $\beta = 12.7$. Evolution of (a) the layer radii r_1/r_0, r_2/r_0, r_3/r_0 and (b) n_3, the mole fraction of Si in the melt. In the simulation, $r_0 = 20\,\mu$m, $D_1 = D_f/V_{m12}$, $D_2 = D_f/V_{m23}$ with D_f given by Eq. (18) and $E_d = 253$ kJ mol^{-1}. Time is measured in seconds.

quantity of about 10^{-4}. We assumed that initially, the melt is largely Si with a small amount of Mo. Thus, the initial amount of the two metals in the liquid phase is fixed to

$$N'_{\mathrm{Si}}(t=0) = (\xi + 0.01)\frac{4\pi r_0^3}{3V_m}; \quad N'_{\mathrm{Mo}}(t=0) = 0.01 \times N'_{\mathrm{Si}}(t=0)$$

The parameter ξ is the stoichiometric coefficient of the initial mixture Mo + ξSi. If it is not specified, we take $\xi = 2$ that ideally corresponds to the formation of pure $MoSi_2$ compound.

4.1. Constant temperature field

We first consider case in which the particle is subjected to a constant temperature field $T = 1900$ K. We suppose that the two diffusion coefficients of Si in $MoSi_2$ and Mo_5Si_3 are the same $D_1 = D_f/V_{m12}$ and $D_2 = D_f/V_{m23}$ where D_f is given by (18) with $E_d = 309$ kJ mol^{-1}. As shown in Fig. 5, we observe the transient formation of a Mo_5Si_3 layer. For an initial particle size $r = 5\,\mu$m, the time for complete conversion of Mo into $MoSi_2$ is about 2.9 s and the maximum of Mo_5Si_3 layer thickness does not exceed 4% of the particle radius. For a smaller value of the activation energy, $E_d = 253$ kJ mol^{-1}, the time of complete conversion is reduced to 0.85 s but the layer thickness is about the same. As expected, we note a drastic change in the time scale of the process as a function of the diffusion characteristics.

4.2. SHS temperature pulse

The typical SHS profile the system is subjected to in our simulations is shown in Fig. 4 ($\beta = 12.7$). The temperature starting above the melting temperature of Si quickly reaches its maximum value and slowly decreases to its initial value in less than 10 s, as is the case in many SHS systems. Fig. 6 shows the evolution of the layer radii and the mole fraction, n_3, of Si in the liquid phase outside the reacting solid sphere, under the influence of the thermal pulse (19) produced by the propagation of the reactive front. The simulation shows that an entire particle of Mo of $r_0 = 20\,\mu$m is converted into $MoSi_2$ in less than 2 s. During this transformation, a thin Mo_5Si_3 layer grows and disappears with the completion of the reactive process. Its thickness never exceed 1 μm. For a cooling that follows the SHS temperature profile, there is no reason to observe a final multiphase product with both disilicides. But when the cooling is forced by a sudden quenching, one may observe unreacted Mo core covered by Mo_5Si_3 layer (see for instance [10]).

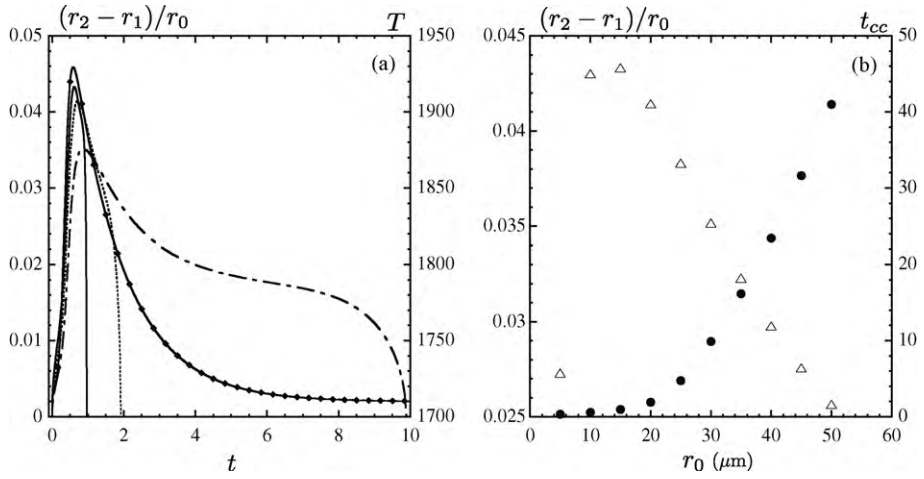

Fig. 7. (a) Time evolution of the Mo_5Si_3 layer thickness (left Y-axis) for different initial particle sizes: $r_0 = 15\,\mu$m (solid line), $r_0 = 20\,\mu$m (dotted line) and $r_0 = 30\,\mu$m (dashed-dotted line). Time evolution of the temperature (right Y-axis – solid line with diamonds). Parameter values: $D_1 = D_f/V_{m12}$, $D_2 = D_f/V_{m23}$ with D_f given by Eq. (18) and $E_d = 253$ kJ mol^{-1}. Time is measured in seconds. (b) Maximum Mo_5Si_3 layer thickness $(r_2 - r_1)/r_0$ (left Y-axis) and time of complete conversion t_{cc} of the Mo solid particle (right Y-axis) as a function of the initial particle size r_0 (μm). Same parameters values as (a).

It is well known that the granulometry of the green mixture influences the microstructure of the final product and by the way the layering process. To study this aspect, we keep all parameters values identical except the initial size of molybdenum particles. The test particle is varied from 5 to 50 μm which are typical particle sizes of commercial powders. The time evolution of the Mo_5Si_3 layer thickness differs significantly for $r_0 = 15\,\mu m$ and $r_0 = 30\,\mu m$ (see Fig. 7a). For $r_0 = 15\,\mu m$, the maximum thickness is less than 1 μm and corresponds to the maximum of the temperature profile. After reaching this value, the layer disappears abruptly with the complete transformation of Mo into $MoSi_2$. For larger initial size particles ($r_0 = 30\,\mu m$), the layer thickness decreases slowly during the cooling of the sample. It seems thus easier to observe a layered microstructure when quenched samples made of larger powders. From the numerical analysis, it is possible to compute two quantities that characterize the reactive process: the time for complete transformation of the Mo particle t_{cc} and the maximum size of the Mo_5Si_3 layer thickness. The time for complete conversion of the Mo particle increases sharply as the initial size increases (see Fig 7b), but the layer thickness never exceeds 4.5% of the initial size (for instance: $\approx 1.2\,\mu m$ for $r_0 = 40\,\mu m$).

We next analyze the effect of the diffusional transport on the morphology at the level of the individual grains. In this preliminary investigation, the main method of analysis is presented. Since the numerical values of the two diffusion coefficients are known only approximately, we have decided to look at the consequences of when one differs from the other by a factor of 2. When more precise data are available, our computer code can easily include the appropriate activation energies and do the simulations. Such detailed work could be investigated in future studies.

The dependence of the evolution of the Mo_5Si_3 layer thickness on the relative values of the diffusion coefficients is shown in detail in Fig. 8. The maximum thickness of the Mo_5Si_3 layer increases with an increase in D_{f1} relative to D_{f2}. In the case that D_{f1} is larger than D_{f2}, the maximum size is reached in the cooling zone of the thermogram. In this opposite case ($D_{f1} < D_{f2}$), the time scale of the overall process is slightly reduced, and the maximum size of the layer is observed when the temperature reaches the combustion temperature and the thickness of the layer is twofold smaller than for $D_{f1} = D_{f2}$. This analysis shows that the intermediate layers may act as a diffusional barrier for the progress of the reaction. For instance, in the case $D_{f1} > D_{f2}$, the diffusion of Si in the first layer around Mo is more efficient and the formation of Mo_5Si_3 is favoured. In the case $D_{f1} < D_{f2}$, Si diffuses rapidly in the second layer and the Mo_5Si_3 produced is quickly converted into $MoSi_2$ at interface II. Through this analysis, it becomes obvious that the diffusional transport in the intermediate layer influences the morphology at the level of the individual grains.

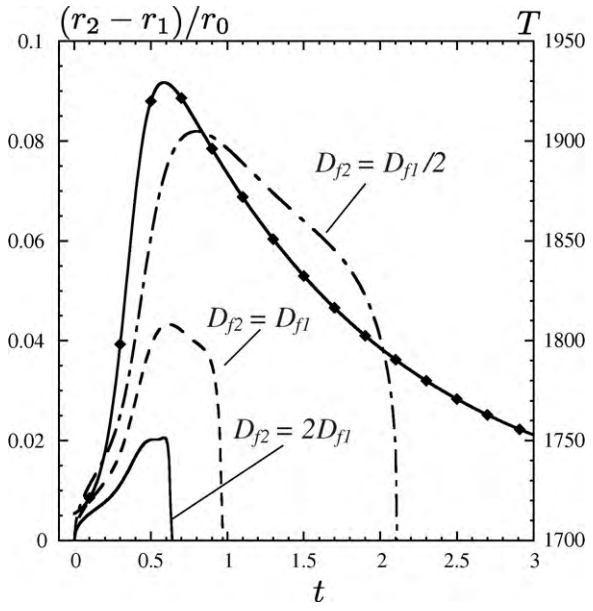

Fig. 8. Time evolution of the Mo_5Si_3 layer thickness (left Y-axis) for different ratio of the diffusion coefficients: $D_{f2} = 2D_{f1}$ (solid line), $D_{f2} = D_{f1}$ (dashed line) and $D_{f2} = D_{f1}/2$ (dashed-dotted line). Time evolution of the temperature (right Y-axis – solid line with diamonds). Parameter values: $r_0 = 15\,\mu m$, $D_1 = D_f/V_{m12}$, $D_2 = D_f/V_{m23}$ with D_f given by Eq. (18) and $E_d = 253\,kJ\,mol^{-1}$. Time is measured in seconds.

The experimental study carried out in [12] and [17] on the formation of disilicides by SHS shows that the stoichiometry of the initial mixture $Mo + \xi Si$ significantly influences the nature of end-product phases. For a coefficient ξ ranging from 2 to 0.6, a reaction front is expected to self-propagate in the system since the combustion temperature is larger than 1800 K. In the simulation, we can easily modify the value of the parameter ξ of the green mixture and test the predictions of our model. As soon as ξ is slightly less than 2 ($\xi = 1.9$), we observe the persistence of a Mo_5Si_3 layer after the completion of the process. Fig. 9 shows the evolution of the radii for $\xi = 1.8$. At a particular time, at which the temperature reaches its maximum value, the evolution of the system drastically changes. The radius r_2 of the Mo_5Si_3 layer smoothly increases and the outermost layer remains practically invariant while the Mo solid particle continue to be consumed to produce Mo_5Si_3. The amount of Si becomes too small to produce $MoSi_2$ at interface II. For lower val-

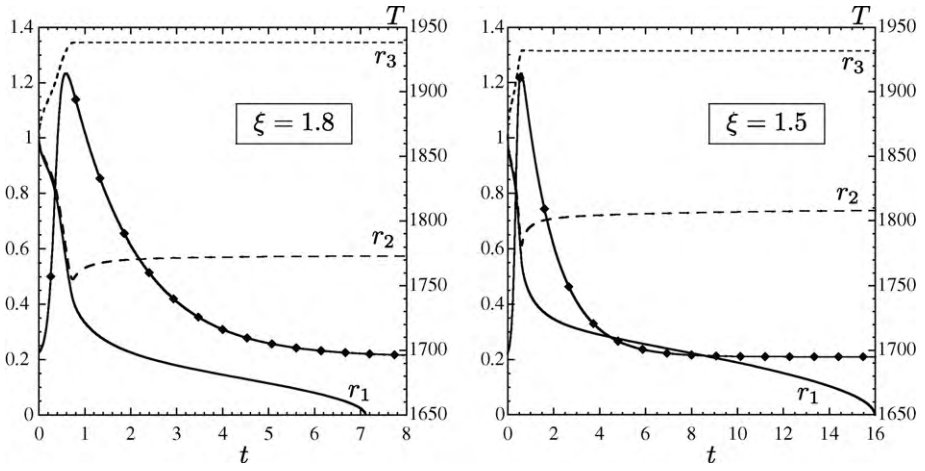

Fig. 9. Evolution of layer radii (left Y-axis) r_1/r_0, r_2/r_0, r_3/r_0 for a green mixture $Mo + \xi Si$, with $\xi = 1.8$ and with $\xi = 1.5$. Time evolution of the temperature (right Y-axis – solid line with diamonds). Parameter values as Fig. 6 except $r_0 = 15\,\mu m$ and $T_0 = 1695\,K$.

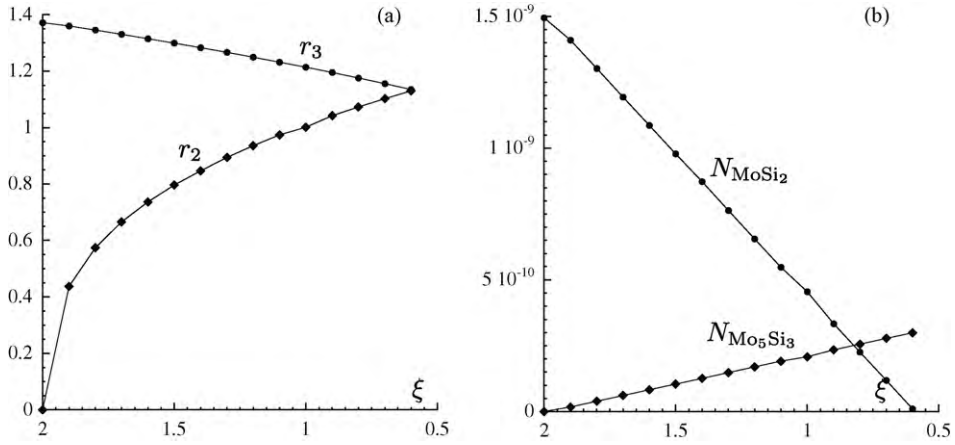

Fig. 10. (a) Radius r_2/r_0 of the Mo_5Si_3 layer (diamonds) and of the outermost layer r_3/r_0 (bullets) as a function of the initial composition of the mixture $Mo + \xi Si$ after the completion of the process. (b) Final number of moles in the solid phase after completion. Parameters values as in Fig. 9.

ues of ξ (see Fig. 9 for $\xi = 1.5$), the decrease of r_2 stops at a higher value and then slowly grows during the cooling. The time for completion may take more than 30 s for stoichiometric coefficient close to unity. The reactive transformation of Mo is characterized by two time scales: one corresponding to the development of a thin Mo_5Si_3 layer during the heating step, then the process is inverted and the amount of Mo_5Si_3 increases with the gradual disappearance of the Mo particle. It is thus not surprising that unreacted Mo core surrounded by Mo_5Si_3 is frequently observed for off-stoichiometric green mixtures.

In Fig. 10a, we show the final Mo_5Si_3 layer thickness as a function of ξ and the final size of the solid product after completion of the process. For $\xi = 0.6$, as expected, only Mo_5Si_3 is formed. In Fig. 10b, the amount of moles of the two silicides in the final product is given as a function of the stoichiometric coefficient of the initial mixture. This amount is just given by the volume of the layer divided by the molar volume of the compound. As expected, for $\xi \approx 1$, we get the same amount of the two phases. Thus, we see how the composition of the green mixture is correlated with the layer structure of the synthesized micro-spheres.

5. Conclusion

The model presented in this article captures many aspects of a complex diffusion-reaction process taking place under typical time-dependent temperature encountered in self-propagating high-temperature synthesis. The model is based on the phase diagram of the bimetallic system, Si and Mo in this case, and the equations of the system do not involve partial differential equations. The parameters used in the model are all experimentally measurable, though not always readily so; thus, through this model, final microstructures of the SHS product is related to the basic reaction and transport processes of the system. For cases in which there are more than two phases of the bimetallic compounds, the model can be extended to systems that have more than two layers of intermetallic compounds.

Our model predicts the dynamical behavior, such as the rate and thickness of the layer growth and relates it to the SHS temperature profile and the composition of the green mixture. As shown in Fig. 7(b), it can relate the initial size of the Mo spheres to the time it takes for the Mo spheres to completely convert to product. Of particular interest is the relation between the microstructure of the Mo particle and the stoichiometric parameter, ξ, shown in Figs. 9 and 10. This relationship enables us to correlate theoretical predictions to the experimental study of the layered microstructure obtained through SHS.

Under controlled conditions, such as isothermal reaction conditions followed by quenching, the correlation between the system parameters, such as the reaction and diffusion rates, and the layer formation in the Mo spheres can be investigated with more detail. Since the time profile of the temperature can be set independently in this model, such isothermal studies are excellent ways of comparing theory with experiment.

In addition to the microstructure of the solid Mo spheres, which remain solid during the process, the model also predicts the overall composition of the liquid phase. However, the model does not include the process of nucleation and growth in the liquid phase if the temperature decreases to a level at which the liquid phase begins to solidify. By knowing the ratio of the moles of Mo to Si, if it is close to 1:2, we could say most of the Mo that diffuses into Si melt will become $MoSi_2$, but such statements are only general and say nothing about the microstructure of the solidifying melt. This part of the process is very complex and requires much more sophisticated modeling. Such an extension of the model including the two possible mechanisms of formation of $MoSi_2$ would be a significative improvement in the understanding of $MoSi_2$ synthesis. A first attempt in this way has been proposed in [28].

Finally, we would like to remark about the temperature field: The assumed temperature field is the “mean field” that propagates through the system so that every microsphere is subject to a “typical” temperature profile. A wide variety of non-isothermal time-dependent conditions can be specified. In particular, the model is particularly appropriate to describe experiments with electrically heated wires in which the temperature profile is imposed. For modeling combustion processes, the shape of the temperature profile must be chosen with care so as to match that generated by the exothermic process. With parameters used in our temperature profile, we can generate a profile appropriate to the desired conditions. The case presented in our study assumes a temperature profile that remains above the melting point of Si for the duration of the simulation. Future development of the theory is precisely aimed at formulating a self-consistent temperature method in which the shape of the temperature profile and the exothermic reaction are made self-consistent.

Acknowledgments

This work has been partly supported by the Chemistry Department and the “Centre de dynamique des systèmes complexes” of the University of Burgundy.

Appendix A.

In this appendix, we discuss the assumptions leading to the expression (4) for the reaction rate R_1 at the interface Mo/Mo_5Si_3 due to an excess of Si with respect to its equilibrium value. From basic thermodynamics of irreversible processes [42], it follows that the rate of reaction $5Mo + 3Si \rightarrow Mo_5Si_3$ is proportional to the affinity $\mathcal{A} = 5\mu_{Mo} + 3\mu_{Si} - \mu_{Mo_5Si_3}$. The chemical potential μ_x of x can be written as $\mu_x = \mu_x^0 + RT\ln(a_x)$ where a_x is the activity and μ_x^0 is the standard-state chemical potential. Equilibrium corresponds to $\mathcal{A} = 0$.

The inner core is pure Mo and Mo_5Si_3 is the major component of the adjacent layer to the interface. The chemical potential of Mo and Mo_5Si_3 does not change as much as the chemical potential of the minor component Si in the Mo_5Si_3 layer. The affinity A depends mostly on the excess of Si and, close to equilibrium, $\mathcal{A}$ is simply proportional to $a_1 - a_{1eq}$ where a_1 is the activity of Si at interface I.

Since the activity a_k is equal to $\gamma_k n_k$ in which n_k is the mole fraction and γ_k the activity coefficient, which for ideal systems, equals 1. In order to simplify the theory, we shall assume $\gamma_k \approx 1$. This leads immediately to Eq. (4).

A similar derivation is applicable for interface II ($Mo_5Si_3/MoSi_2$).

Appendix B.

In this appendix, we give some basics about the diffusion transport process which are useful in the framework of our modeling. Following Fick's law, diffusion current is expressed in terms of the concentration gradient and the corresponding diffusion coefficient D_f has units of $m^2\,s^{-1}$. The diffusion current can also be expressed as the gradient of mole fraction since, at least in dilute solutions, the concentration c is directly related to the mole fraction by the relation $c = n/V_m (\mathrm{mol\,m^{-3}})$ where V_m is the molar volume. Hence we have

$$J = -D_f \frac{\partial c}{\partial r} = -\frac{D_f}{V_m}\frac{\partial n}{\partial r} = -D\frac{\partial n}{\partial r} \tag{B.1}$$

where $D = D_f/V_m$ has units of $\mathrm{mol\,m^{-1}\,s^{-1}}$.

In a spherical symmetry, the condition for a stationary diffusion process implies that the current times the surface remains constant $4\pi r^2 \times J =$ constant for any value of r. Since J is given by Eq. (B.1), we get the expression for the mole fraction profile $n(r) = A/r + B$ where the constant values A and B are fixed by the boundary conditions $n = n_1$ at r_1 and $n = n_2$ at r_2:

$$A = \frac{n_1 - n_2}{r_1^{-1} - r_2^{-1}}$$

It is then easy to compute the explicit expression of the diffusion current [43]. For instance, at the interface I, we have

$$J = -D_1 \left.\frac{\partial n}{\partial r}\right|_{r_1} = D_1\frac{A}{r_1^2} = -D_1\frac{r_2}{r_1}\frac{n_2 - n_1}{r_2 - r_1} \tag{B.2}$$

The negative sign implies that the current is flowing toward the center if $n_2 > n_1$ since we have used the standard convention $\mathbf{J} = J\mathbf{1_r}$ where $\mathbf{1_r}$ is the unit vector in the direction of increasing r. In the main text (see Eq. (10)), we introduce a positive J_1 for the flow toward the center to avoid any ambiguity.

Appendix C.

We present here the nomenclature of the model:

N'_{Mo}	amount (moles) of Mo in the melt
N'_{Si}	amount (moles) of Si in the melt
N_{MoSi_2}	amount (moles) of $MoSi_2$
$N_{Mo_5Si_3}$	amount (moles) of Mo_5Si_3
N_{Mo}	amount (moles) of Mo in the solid sphere
V_{mMo}	molar volume of solid Mo
V_{m12}	molar volume of Mo_5Si_3
V_{m23}	molar volume of $MoSi_2$
a_1	activity of Si at interface I = n_1 = mole fraction at interface I
a_{1eq}	equilibrium activity of Si at interface I = n_{1eq} = equilibrium mole fraction at interface I
a_2	activity of Si at interface II = n_2 = mole fraction at interface II
a_{2eq}	equilibrium activity of Si at interface II = n_{2eq} = equilibrium mole fraction at interface II
a_3	activity of Si at interface III = n_3 = mole fraction at interface III
a_{3eq}	equilibrium activity of Si at interface III = n_{3eq} =equilibrium mole fraction at interface III.
D_1	diffusion coefficient of Si in the Mo_5Si_3 phase
D_2	diffusion coefficient of Si in the $MoSi_2$ phase
J_1	diffusion current at interface I
J_2	diffusion current at interface II
J_3	diffusion current at interface III

References

[1] See for instance Mater. Sci. Eng. A 155(1–2) (1992).
[2] Y.J. Jeng, B.J. Lavernia, J. Mater. Sci. 29 (1994) 2557.
[3] N.S. Stoloff, Mater. Sci. Eng. A 261 (1999) 169.
[4] J. Subrahmanyam, J. Am. Ceram. Soc. 76 (1) (1993) 226.
[5] C.D. Wirkus, D.R. Wilder, J. Am. Ceram. Soc. 49 (4) (1966) 173.
[6] W.Y. Lin, L.Y. Hsu, R.F. Speyer, J. Am. Ceram. Soc. 77 (5) (1994) 1162.
[7] J. Karch, R. Birringer, H. Gleiter, Nature 330 (1997) 556.
[8] J.J. Petrovic, Mater. Sci. Eng. A 192/193 (1995) 31;
J.J. Petrovic, A.K. Vasudevan, Mater. Sci. Eng. A 261 (1999) 1.
[9] I.J. Shon, Z.A. Munir, K. Yamazaki, K. Shoda, J. Am. Ceram. Soc. 79 (1996) 1875.
[10] C. Cabouro, S. Chevalier, E. Gaffet, D. Vrel, N. Boudet, F. Bernard, Acta Mater. 55 (2007) 6051.
[11] A.R. Sarkisyan, S.K. Dolukhanyan, I.P. Borovinskaya, A.G. Merzhanov, Fizika Goreniya i Vzriva 14 (1978) 49;
A.R. Sarkisyan, S.K. Dolukhanyan, I.P. Borovinskaya, Powder Metall. 6 (1978) 14.
[12] S. Zhang, Z.A. Munir, J. Mater. Sci. 26 (1991) 3685.
[13] S.C. Deevi, Mater. Sci. Eng. A 149 (1992) 241.
[14] S.C. Deevi, N.N. Thadani, Mater. Sci. Eng. A 192 (1995) 604.
[15] S.W. Jo, G.W. Lee, J.T. Moon, Y.S. Kim, Acta Mater. 44 (1996) 4317.
[16] Ch. Gras, E. Gaffet, F. Bernard, Intermetallics 14 (2006) 521.
[17] C.L. Yeh, W.H. Chen, J. Alloys Compd. 438 (2007) 165.
[18] A.G. Merzhanov, I.P. Borovinskaya, Dolk. Akad. Nauk. SSSR 204 (1972) 366.
[19] Z.A. Munir, Ceram. Bull. 2 (1988) 342.
[20] J.J. Moore, H.J. Feng, Prog. Mater. Sci. 38 (1995) 272.
[21] F. Charlot, E. Gaffet, F. Bernard, B. Zeghmati, J.C. Niepce, Mater. Sci. Eng. A 262 (1999) 279.
[22] V. Gauthier, C. Josse, F. Bernard, E. Gaffet, J.P. Larpin, Mater. Sci. Eng. A 264 (1999) 117.
[23] Ch. Gras, D. Vrel, E. Gaffet, F. Bernard, J. Alloys Compd. 314 (2001) 240.
[24] F. Bernard, E. Gaffet, Int. J. SHS 10 (2001) 109.
[25] A.G. Merzhanov, J. Mater. Chem. 14 (2004) 1779.
[26] H.A. Chatilyan, L.H. Arakelyan, S.L. Kharatyan, Defect Diffus. Forum 237–240 (2005) 867.
[27] S.L. Kharatyan, H.A. Chatilyan, A.S. Mukasyan, D.A. Simonetti, A. Varma, AIChE J. 51 (2005) 261.
[28] G.S. Galstyan, H.A. Chatilyan, A.G. Kirakosyan, S.L. Kharatyan, A.S. Mukasyan, A. Varma, Defect Diffus. Forum 237–240 (2005) 873.
[29] E.A. Nekrasov, V.N. Tkachenko, A.E. Zakirov, Combust. Sci. Technol. 91 (1993) 207.
[30] H. Mehrer, Diffusion in Solids, Springer, 2007.
[31] T.B. Massalski, H. Oamoto, P.R. Subramaniam, Binary alloy phase diagrams, vol. 2, Second edition, ASM international, M.P., OH, 1990.
[32] Y. Buyn, J.-K. Yoon, G.-H. Kim, J.-S. Kim, C.S. Choi, Scripta Mater. 46 (2002) 537.
[33] H.A. Chatilyan, S.L. Kharatyan, A.B. Harutyunyan, Mater. Sci. Eng. A 459 (2007) 227.
[34] F. Baras, D. Kondepudi, J. Chem. Phys. B 111 (2007) 6457.
[35] P.C. Tortorici, M.A. Dayananda, Mater. Sci. Eng. A 261 (1999) 64.
[36] S.W. Chae, C.H. Son, Y.S. Kim, Mater. Sci. Eng. A 279 (2000) 111.

[37] P.C. Tortorici, M.A. Dayananda, Scripta Mater. 38 (1998) 1863.
[38] P.C. Tortorici, M.A. Dayananda, Metall. Mater. Trans. A 30 (1999) 545.
[39] F. Christian, T. Narita, Mater. Trans. JIM 39 (1998) 658–662.
[40] A. Hibino, Int. J. SHS 8 (1999) 13.
[41] F. Baras, J. Alloys Compd. 455 (2008) 113.
[42] D.K. Kondepudi, I. Prigogine, Modern Thermodynamics: From Heat Engines to Dissipative Structures, John Wiley, New York, 1998.
[43] B. Delmon, Introduction à la Cinétique Hétérogène, Technip, Paris, 1969.